

Supplementary Information

Tom Ellaby, Aakash Varambhia, Xiaonan Luo,
Ludovic Briquet, Misbah Sarwar, Dogan Ozkaya,
David Thompsett, Peter Nellist and Chris-Kriton Skylaris

July 2020

1 Strain calculations

While we need to use a projected grid to construct the strain tensor, it is clear there are problems with this method. The major issue is that strain is accumulated as atoms get further from the reference position. As an example, if a nanoparticle was uniformly strained by 1% (all nearest neighbour distances reduced by 1%), this method would show 0% strain for the reference point, 1% for each of its nearest neighbours, then 2% for the next atoms along the lattice basis directions, and so on. In practice, this has the effect of exaggerating the strain of the outermost layers of the nanoparticles, since they are furthest from the reference point in the centre.

Here, the approach we have adopted is to fit the grid using a least squares method over the whole nanoparticle, which we describe in more detail below. By doing this, we avoid biasing the centre of the nanoparticle as much. While our least squares approach does help mitigate the issues that we have highlighted with a projected grid method, it cannot completely eliminate them, as choosing an averaged reference point does not fully remove the bias towards atoms that are closer to it.

1.1 Strain and effective lattice parameter measurements from ADF images (2D)

In order to calculate the strain, a peak finding routine was used to find the atomic column positions. This was followed with a centre of mass refinement and 2D Gaussian fitting [1], the result of which is shown in figure 1. At the surface (2D projection), only atoms with the least movement were chosen for the strain analysis. Each image frame was checked to see whether atom hopping occurred in-between frames and whether there were any missing columns on the surface. For instance in figure 1, we can see that there appears to be a whole plane that has been ignored in the analysis, however, this is deceptive as we are looking at a cumulatively summed image from several frames.

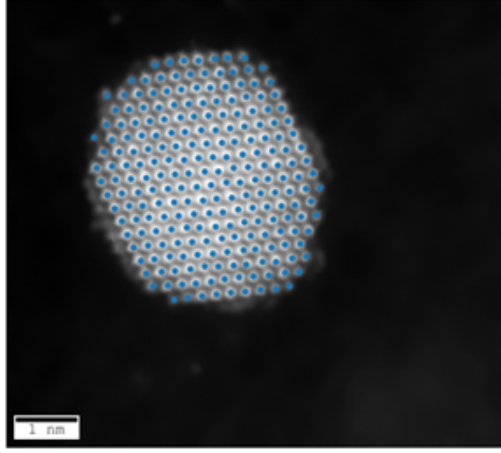


Figure 1: Fitted peaks from the routine used to find the atomic column positions.

Figure 2 shows the difference between the 1st frame and the 20th frame during image acquisition. We can see that some of the surface atoms have moved significantly between the frames and there are also indications of beam damage. The surface layers of these nanoparticles are known to play an important role in catalysis and thus uncertain measurements from the hopping atoms were removed from the peak fitting routine.

Once the peak positions of the atomic columns were confidently defined, the centre of the nanoparticle was determined by calculating the geometric centre of the column position point cloud. For the atom in the centre, a nearest neighbour search was conducted in 6 directions to obtain the fcc [110] neighbours. Using the nearest neighbours, sets of vector pairs were calculated in every direction. One of the vector pairs is shown in figure 3a.

For each atomic column, a directional nearest neighbour search is performed along the directions defined by the vector pair. This is shown in figure 3b. In the special case where the directional search yields no atomic columns, i.e. vacuum in the vector direction (at the edge of the nanoparticle), a directional search in the opposite direction is carried out, also shown in figure 3b. If the directional search in the opposite direction also yields vacuum such as the single atomic column with no directional neighbours along the vector pair we have chosen, then a two nearest neighbour atoms search is conducted.

Using the inner vectors from the second layer onward from the outside of nanoparticle a reference grid was constructed. The first layer was ignored when creating this grid due to the directional search for some columns having vectors that are in the opposite direction leading to double counting, in some cases the vectors also have a different rotation and belong to another basis pair. These inner vectors are averaged to obtain a general vector system for the particle that is used to create a reference grid for the nanoparticle. Once created, the

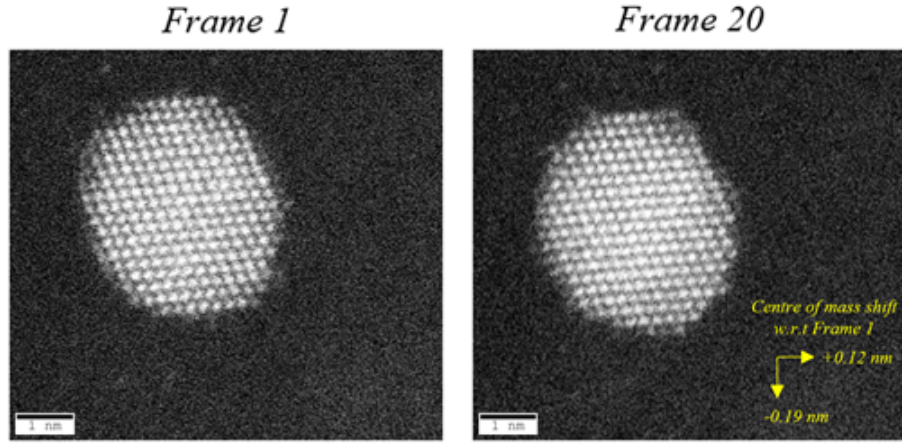


Figure 2: Surface atom hopping and damage comparison between the 1st frame and the 20th frame of a nanoparticle during experimental imaging.

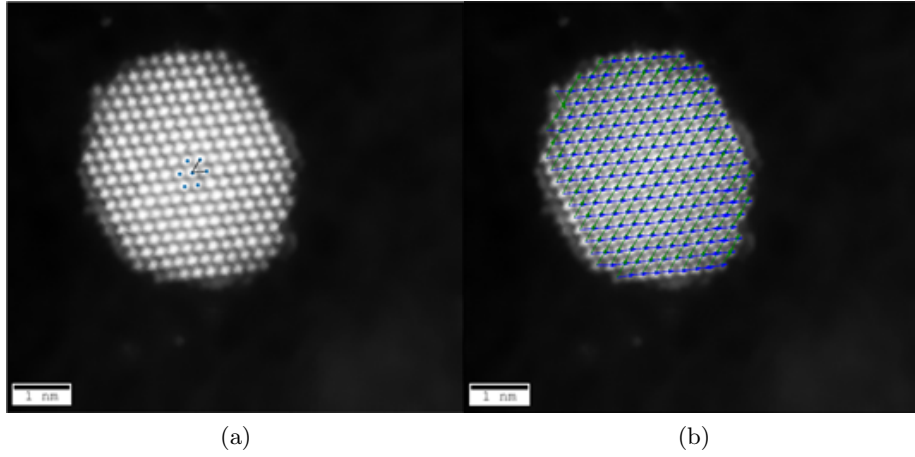


Figure 3: A set of vectors with the origin as the centre atom (a), and the directional nearest neighbour search along these vector directions (b).

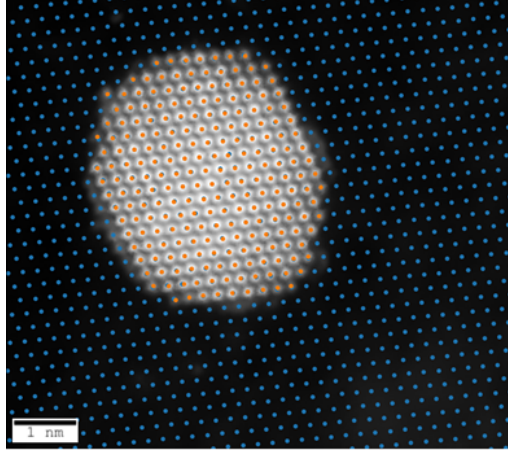


Figure 4: The nanoparticle atomic column positions (orange) overlaid with a best fit grid obtained from a least square fit refinement (blue).

reference grid it is overlaid on top of the atomic positions of the nanoparticle and a least squares refinement is carried out. In this refinement procedure, the grid is free to translate, rotate and expand/contract. This procedure means that the grid that is created is a best fit grid for the whole nanoparticle, shown in figure 4.

The nearest neighbour vectors between the reference grid and the measured atomic column positions provide the displacement vectors of the atomic columns with respect to the nanoparticle average. In order to calculate the strain components the peak-pair formulation was used [2, 3], shown in figure 5.

In the peak-pair formulation, the blue atom represents the observed atomic column we want to compute the strain for, whereas the orange and yellow atoms are the nearest neighbour and reference positions respectively. From the vector average atomic column positions in Figure 4 that were used to create the reference grid, it is possible to get a localised reference at each atomic column. Using this localised reference and the observed nearest neighbour atomic column positions it is possible to calculate the strain tensors as shown by (1).

$$\begin{bmatrix} \varepsilon_{xx} & \epsilon_2 \\ \epsilon_1 & \varepsilon_{yy} \end{bmatrix} = \begin{bmatrix} a_x & a_y \\ b_x & b_y \end{bmatrix}^{-1} \begin{bmatrix} u_x & u_y \\ v_x & v_y \end{bmatrix} \quad (1)$$

Once the strain tensors have been computed the shear forces can be calculated using (2)

$$\varepsilon_{xy} = \frac{1}{2} (\epsilon_1 + \epsilon_2) \quad (2)$$

The rotational component can be calculated as

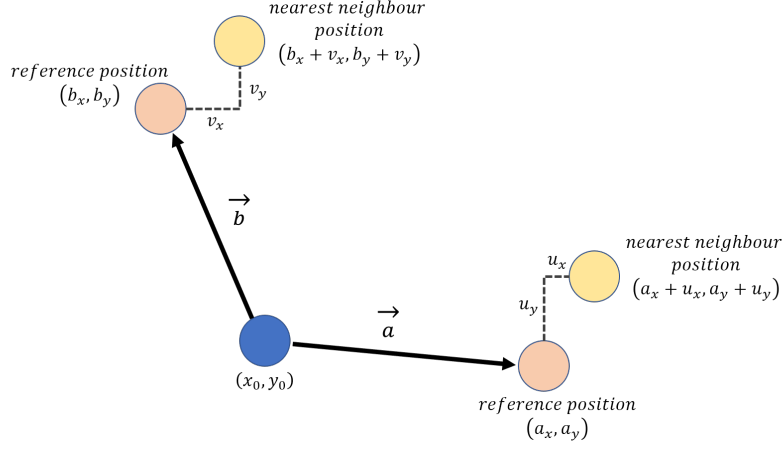


Figure 5: Peak-pair method schematic for computing the strain tensor

$$\omega_{xy} = \frac{1}{2} (\epsilon_1 - \epsilon_2) \quad (3)$$

The change in the cell vector pair area, if we assume a perfect parallelogram, can be calculated as

$$\delta = \epsilon_{xx} + \epsilon_{yy} \quad (4)$$

The change in this cell area could then be compared to a direct measurement from the ADF image neighbouring columns for a consistency check. With this procedure it is possible to directly relate the vector cell contraction, expansion, shear and rotation to an effective lattice parameter measurement. Here the effective lattice parameter was calculated by relating the area of the parallelogram to the respective fcc [110] cell projection area.

As each atom in a column experiences forces from neighbouring atoms, we calculated the effective lattice parameter and strain tensor components for all possible vector pair directions. These measurements were then averaged to obtain the final strain and effective lattice parameter measurements for a nanoparticle. This also means that we have defined the effective lattice parameter of an atom as an average distance measurement calculated from an area of neighbouring columns.

2 Electronic structure and descriptors

Performing DFT single point calculations also gives us access to electronic structure information of our systems. There are many descriptors based on these properties, and here we assess how the presence of Co in our annealed structures might affect O and CO binding. The local, d-projected density of states

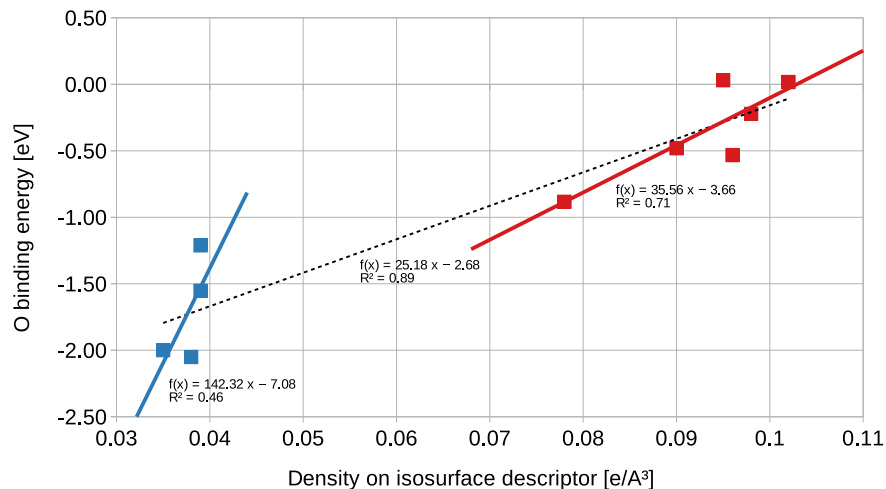


Figure 6: Electron density based descriptor vs oxygen binding energy for atop sites on a 202 atom Pt_3Co truncated octahedral nanoparticle. Co and Pt sites are plotted in blue and red, respectively. [add key]

is a well known and well used descriptor the binding of adsorbates on metal surfaces.

To assess the applicability of our descriptors, we have performed binding energy calculations for oxygen ligands on various sites on a 202 atom truncated octahedral nanoparticle with a random distribution of Pt and Co in a 3:1 ratio. These binding energies were calculated using full geometry relaxations, meaning that the isolated nanoparticle geometry was allowed to relax, and the full system with the oxygen ligand was also fully relaxed.

We have compared these binding energies with a descriptor based on the electron density and the electrostatic potential, first described by Aarons et al. [4], and used in our previous work on titania supported nanoparticles [5]. It is calculated by constructing an isosurface of the electrostatic potential around the nanoparticle, and then finding the electron density across that surface. Binding strength of a site is then related to the value of the descriptor local to that site.

For alloyed systems, electronic descriptors such as this have an advantage over geometric ones like generalised coordination number [6] since they require no extra parametrisation to account for different chemical species. Further, when using geometric descriptors for Pt shell nanoparticles, they will only be sensitive to strain and any reconstruction of the nanoparticle facets, etc., while the changes in electronic structure may also be important.

Figure 6 shows the correlation between binding energy and the descriptor. The descriptor shows a clear distinction between Co and Pt atoms, resulting two clusters of points, though the difference in calculated binding energy does not jump by as much. Within the Co cluster, the descriptor does not appear to

be particularly sensitive, while for the Pt cluster it performs significantly better. Fortunately, since the systems of greatest interest are Pt shell structures, the Pt sites are the more important ones.

References

- [1] Magnus Nord, Per Erik Vullum, Ian MacLaren, Thomas Tybell, and Randi Holmestad. Atomap: A new software tool for the automated analysis of atomic resolution images using two-dimensional Gaussian fitting. *Advanced Structural and Chemical Imaging*, 3(1):9, February 2017.
- [2] A. De Backer, K. H. W. van den Bos, W. Van den Broek, J. Sijbers, and S. Van Aert. StatSTEM: An efficient approach for accurate and precise model-based quantification of atomic resolution electron microscopy images. *Ultramicroscopy*, 171:104–116, December 2016.
- [3] Pedro L. Galindo, Slawomir Kret, Ana M. Sanchez, Jean-Yves Laval, Andrés Yáñez, Joaquín Pizarro, Elisa Guerrero, Teresa Ben, and Sergio I. Molina. The Peak Pairs algorithm for strain mapping from HRTEM images. *Ultramicroscopy*, 107(12):1186–1193, November 2007.
- [4] Jolyon Aarons, Lewys Jones, Aakash Varambhia, Katherine E. MacArthur, Dogan Ozkaya, Misbah Sarwar, Chris-Kriton Skylaris, and Peter D. Nellist. Predicting the Oxygen-Binding Properties of Platinum Nanoparticle Ensembles by Combining High-Precision Electron Microscopy and Density Functional Theory. *Nano Lett.*, 17(7):4003–4012, July 2017.
- [5] Tom Ellaby, Ludovic Briquet, Misbah Sarwar, David Thompson, and Chris-Kriton Skylaris. Modification of O and CO binding on Pt nanoparticles due to electronic and structural effects of titania supports. *J. Chem. Phys.*, 151(11):114702, September 2019.
- [6] Federico Calle-Vallejo, José I. Martínez, Juan M. García-Lastra, Philippe Sautet, and David Loffreda. Fast Prediction of Adsorption Properties for Platinum Nanocatalysts with Generalized Coordination Numbers. *Angewandte Chemie International Edition*, 53(32):8316–8319, 2014.